Journal of Sustainable Civil Engineering and Technology
e-ISSN: 2948-4294 | Volume 3 Issue 1 (March 2024), 90-102
https://joscetech.uitm.edu.my

Quantifying the Efficacy of Retrofitting Slabs Under Local Blast Loads through Numerical Analysis using Polyurea-Infused Woven Glass Fiber Mesh Composites

Muhammad Nuzulul Furqan[1*], **Sofia W Alisjahbana**[1], **Muhammad Daffa Fachrur Reza**[1]

[1]Fakultas Teknik dan Ilmu Komputer, Universitas Bakrie, Jakarta, Indonesia

*Corresponding author: 2023673258@student.uitm.edu.my

Received: 19 January 2024/ Accepted: 12 March 2024/ Published online: 29 March 2024

Abstract

Terrorists now frequently use explosive attacks to carry out assaults. They frequently utilize car bombs, luggage bombs, or suicide bombs to target key buildings, creating fear and drawing public attention. The specimens used consist of semi-rigid slabs with varying thicknesses of 15 cm, 18 cm, and 20 cm. Two models were considered: one with additional reinforcement using polyurea-infused woven glass fiber mesh composites and another without any additional reinforcement. These slabs were subjected to blast loads. Numerical analysis was conducted using Wolfram Mathematica software. When polyurea-infused woven glass fiber mesh composites were used as reinforcement, slabs of decreasing thickness showed a big rise in their resistance to blast loads. This demonstrates the effectiveness of this material in enhancing slab performance under blast conditions. For example, when extra retrofitting using polyurea-infused woven glass fiber mesh composites was done at the same thickness (15 cm), a big drop was seen—a drop of 97.61%. Similarly, at a thickness of 18 cm, a decrease of 30.48% was experienced, while at a thickness of 20 cm, the reduction reached 70.40%.

Keywords: Blast load; Retrofitting; Polyurea-infused woven glass fiber mesh composites

1. Introduction

Nowadays, explosive attacks have become a leading way for terrorists to carry out attacks, where they frequently use car bombs, luggage bombs, or suicide bombs to attack key buildings to create public fear and focus. These bombs pose a severe threat to the safety of the key building and the people in it because of the structural collapse and scattering of explosive fragments. For these reasons, some new key buildings under construction have already considered the hazards caused by the blast wave, e.g., traditional concrete instead of ultrahigh-performance concrete or fiber-reinforced concrete. However, for most old buildings, especially those built in the last century, seeking proper structural retrofitting techniques is a practical approach to upgrading blast resistance against explosive terrorist attacks. Many approaches have been used as retrofitting techniques against blast loading. Some of the traditional methods (e.g., attaching extra structural members or steel skin façades (Ding et. al., 2016), increasing the sectional area of the structural members, etc.) were used to upgrade structures over the last two decades. However, these techniques effectively increase the strength and stiffness of the structure and add extra mass to the structure. However, these methods are undesirable from the perspectives of construction cost and usable space elimination (Nam et. al., 2010). Moreover, this method generally does not significantly increase the overall structural resistance against blast loads (ASCE, 1999), and concrete spalling and fragmentation also cannot be eliminated (Guo et. al., 2017). Therefore, less expensive and more convenient fiber-reinforced polymer (FRP) sheets or plates with high strength and stiffness are gradually used as surface attachments to retrofit specified areas (Pham & Hao, 2016). In the event of an explosion, FRP

can enhance structural members out-of-plane bending strength, stop fragmental debris spalling, and prevent the total failure of structures (Chundawat et. al., 2018). However, most FRP retrofits have some drawbacks, including premature failure due to debonding and delamination, as witnessed in full-scale blast tests (Maji et. al., 2008).

The steady-state response of moving loads on beams supported by elastic foundations was studied by J. T. Kenney. Empirical methods were used in previous research, but with the rapid technological advancement of finite element methods, numerical-based research has become possible in recent years. Jacob et al. (2004) investigated square-shaped steel plates with varying thickness and length-to-width ratios supported by fixed supports, using experimental results and numerical predictions.

Abdelkrim (2008) examined the influence of explosion pressure duration on other parameters, such as strain rate, showing that including the strain rate effect yields a significantly stiffer response. In their research, they studied the dynamic behavior of orthotropic plates subjected to external explosions. The external explosion was fixed, and dynamic deflection was calculated for various durations and amounts of reinforcement. Their research results indicated that the dynamic response of orthotropic plates depends on the amount of reinforcement and the explosion load's duration (Sofia and Wiratman, 2014).

All numerical calculations in this paper were performed using the *Wolfram Mathematica* computer software, developed by Stephen Wolfram. The research focused on rectangular orthotropic plates placed on a Pasternak foundation with semi-rigid placements. Therefore, the homogeneous system's differential equation solution required the Modified Bolotin Method (MBM), a numerical method for solving various plate equations using trigonometric functions (Alisjahbana, Sofia & Wangsadinata, 2008). The Winkler foundation and continuous medium model cannot realistically depict the interaction mechanism between the beam and the contact medium. Among several basic three-parameter models, the Kerr-type basic model received particular attention as it originates from the well-known two-parameter Winkler-Pasternak basic model, which has had various applications and solutions. In the Kerr-type basic model, the underlying medium is illustrated as consisting of upper and lower spring layers enclosing an uncompressed shear layer. In previous research, soil modeling was generally conducted using the Pasternak and Winkler models.

However, this study attempts to fill the knowledge gap by applying the Kerr model for soil modeling. In addition, in the context of plate modeling, previous research typically used the 'simply supported' approach. Conversely, this study strives to expand our understanding by applying a 'semi-rigid' model for plate modeling. Thus, this study aims to provide new contributions in the field of numerical analysis by applying different modeling techniques.

This paper analyzes the dynamic behavior of rigid pavement plates due to local explosion loads with semi-rigid placement on a Kerr foundation. This is done to understand the behavior of plates with semi-rigid placement on the Kerr foundation. Variations in plate thickness and soil type were carried out to determine the dynamic response on the plate that would arise due to the local blast load.

Zhang, et. al., (2023) mentioned a paper to discuss the utilization of composites consisting of polyurea-infused woven glass fiber mesh as well as the measurement of retrofitting slabs under local blast loads. Ibrahim & Metwally (2023) mentioned in the paper that a technique involving the use of polyurea-infused woven glass fiber mesh is implemented to prevent fragmentation in RC slabs that are exposed to contact explosion. The numerical model proved to be an effective tool for designing solutions to retrofit buildings against blasts.

The objective of this study is to quantify the efficacy of retrofitting reinforced concrete slabs under local blast loads through numerical analysis using polyurea-infused woven glass fiber mesh composites. This will be achieved by conducting a comprehensive numerical analysis to evaluate the performance of the retrofitted concrete slabs under local blast loads.

The specific focus will be on assessing the structural response, deformation characteristics, and capabilities of the polyurea-infused woven glass fiber mesh composites in mitigating the effects of local blast loads on the reinforced concrete slabs. These numerical results may serve as design guidelines for structures under blast loading.

2. Methods

All numerical calculations in this paper were performed using the *Wolfram Mathematica* computer software. The numerical method used in this study has previously been implemented and examined (Sofia and Wiratman, 2014). This research provides a strong foundation for further development in this study.

2.1. Description of the orthotropic plate

The material characteristics of the concrete and the reinforcement properties of the stiffening elements significantly impact the dynamic behaviors of an orthotropic concrete plate with semi-rigid conditions along its edges when exposed to the blast load (S. Alisjahbana and W. Wangsadinata, 2012). The subsequent numerical analysis assumes that the connection between the reinforcing bars and the concrete is ideal.

The dimensions of the concrete plate under investigation in this study are 15 x 7.5 meters, with varying plate thicknesses used, which are 15 cm, 18 cm, and 20 cm. Figure 1 depicts the configuration of the orthotropic concrete plate, showcasing its semi-rigid boundary conditions along the edges. This assembly is subjected to the blast load f(x,y,t).

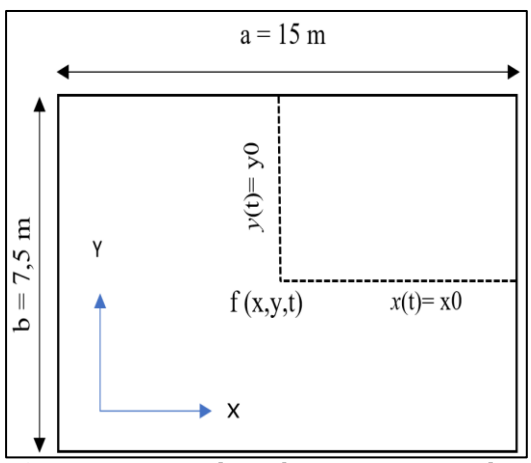

Figure 1. Rectangular orthotropic concrete plate subjected to the blast load at (x0, y0).

The mathematical model of a rectangular orthotropic floor slab that is loaded with blast loads has a length in the x-direction of a, a length in the y-direction of b, and a thickness of the slab h. By using the classic thin plate theory, the deflection of orthotropic slabs is expressed by the differential equation as follows:

$$Dx\frac{\partial^4 w(x,y,t)}{\partial x^4} + 2B\frac{\partial^4 w(x,y,t)}{\partial x^4 \partial^4} + Dy\frac{\partial^4 w(x,y,t)}{\partial y^4} + \gamma.h\frac{\partial w(x,y,t)}{\partial t^2} = p(x,y,t) \quad (1)$$

Where w(x,y,b) is a deflection function based on function (position and time) and p(x,y,t) is a load function based on function (position and time).

2.2. Description of Kerr Foundation

The plate is subjected to a general dynamic load p(x, y, t) which moves at a constant velocity, and it is supported by a Kerr foundation with spring stiffness moduli k_1, k_2, and the shear modulus of the shear layer G_s. This modeling is deemed to be the closest approximation or most accurate representation according to field conditions. The Kerr equation can be expressed (Alisjahbana, Sofia and Wangsadinata, Wiratman, 2008) as follows:

$$-\left[1+\frac{k_2}{k_1}\right]\left[Dx\frac{\partial^4 w}{\partial x^4}+2B\frac{\partial^4 w}{\partial x^2\partial y^2}+Dy\frac{\partial^4 w}{\partial y^4}+\rho h\frac{\partial^2 w}{\partial t^2}+\gamma h\frac{\partial w}{\partial t}-p(x,y,t)\right]$$
$$+\frac{G}{k_1}\left[Dx\left(\frac{\partial^6 w}{\partial x^6}+\frac{\partial^6 w}{\partial x^4\partial y^2}\right)+2B\left(\frac{\partial^6 w}{\partial x^4\partial y^2}+\frac{\partial^6 w}{\partial x^2\partial y^4}\right)+Dy\left(\frac{\partial^6 w}{\partial y^6}+\frac{\partial^6 w}{\partial x^2\partial y^4}\right)\right]$$
$$+\frac{G}{k_1}\left(\frac{\partial^2}{\partial x^2}+\frac{\partial^2}{\partial y^2}\right)\left(\rho h\frac{\partial^2 w}{\partial t^2}+\gamma h\frac{\partial w}{\partial t}-p(x,y,t)\right)=k_2 w-Gs\left(\frac{\partial^2}{\partial x^2}+\frac{\partial^2}{\partial y^2}\right) \quad (2)$$

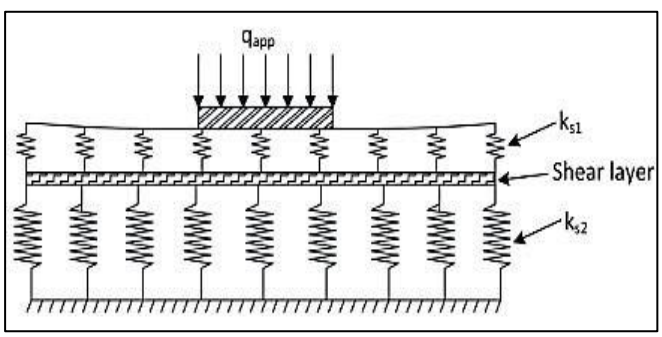

Figure 2. Modeling of the Kerr support layer (A. D. Kerr, 1965)

2.3. Load Function

The explosion load used in this calculation is the explosion load developed by (Sofia and Wiratman, 2014). The positive phase of this load follows an exponential form, while the negative phase utilizes the negative cubic phase function. It was demonstrated in their research that the negative cubic function is the most accurate function for depicting the negative phase of the load.

$$P(t)=\{Pmax\left(1-\frac{t}{tp}\right)e^{-\alpha\frac{t}{tp}}-Pmin(\frac{6.75(t-t_p)}{t_N}\left(1-\frac{1-t_p}{t_N}\right) \quad (3)$$

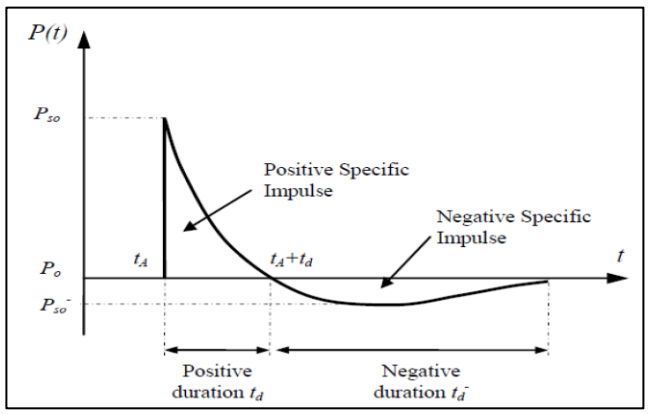

Figure 3. Idealized pressure-time profile for a blast load (Zhang. et. al, 2023)

Choosing the blast load because the type of blast being simulated is a blast above the surface in a real-life situation, the blast load is the most ideal to represent the explosion above the surface as simulated.

2.4. Dynamic Analysis

The rectangular plate model with orthotropic properties features semi-rigid boundary conditions on all four sides, positioned on top of a Kerr foundation layer. The dynamic deflection equation of the orthotropic plate (Equation 2) can be solved by expressing that the solution to the differential equation is a product of the positional function W(x, y) and the temporal function T(t), as follows:

$$w(x,y,t) = \sum_{m=1}^{\infty} \sum_{n=1}^{\infty} W_{mn}(x,y) sin(\omega_{mn} t) \tag{4}$$

When equation (4) is substituted into equation (2) with the conditions of free vibration, the equation is obtained to obtain the value of natural frequency:

$$\begin{aligned} -(k_1+k_2)\left(D_x\frac{\partial^4 w}{\partial x^4} + 2B\frac{\partial^4 w}{\partial x^2 \partial y^2} + D_y\frac{\partial^4 w}{\partial y^4}\right) + G_s\left(D_x\left(\frac{\partial^6 w}{\partial x^6} + \frac{\partial^6 w}{\partial x^2 \partial y^2}\right)\right) \\ + 2B\left(\frac{\partial^6 w}{\partial x^4 \partial y^2} + \frac{\partial^6 w}{\partial x^2 \partial y^4}\right) + D_y\left(\frac{\partial^6 w}{\partial y^6} + \frac{\partial^6 w}{\partial x^2 \partial y^4}\right)) - k_1 k_2 W + G_s(\frac{\partial^2 w}{\partial x^2} + \frac{\partial^2 w}{\partial y^2}) \\ = \rho h {\omega_{mn}}^2 (k_1\left(\frac{\partial^2 w}{\partial x^2} + \frac{\partial^2 w}{\partial y^2}\right) - (k_1+k_2)W) \end{aligned} \tag{5}$$

For rectangular plates with semi-rigid bearings on the x and y sides, the following conditions apply:

$$W(x,y) = 0, \text{ di } x = 0 \text{ and } x = a \tag{6}$$

$$D_x\left(\frac{\partial^2 W}{\partial x^2} + v_y\frac{\partial^2 W}{\partial y^2}\right) = k_{rx}\frac{\partial W}{\partial x}, \text{ di } x = 0 \text{ and } x = a \tag{7}$$

$$W(x,y) = 0, \text{ di } y = 0 \text{ and } y = b \tag{8}$$

$$D_y\left(\frac{\partial^2 W}{\partial x^2}+v_y\frac{\partial^2 W}{\partial y^2}\right)=k_{ry}\frac{\partial W}{\partial y}\text{, di y = 0 and y = b} \tag{9}$$

For a plate with semi-rigid bearings on all four sides, the solution to the position function of the equation of motion that satisfies the boundary conditions can be expressed as follows:

$$W_{mn}=\ A_{mn}\,Sin\left(\frac{m\pi x}{a}\right)Sin\left(\frac{m\pi y}{b}\right) \tag{10}$$

p and q are real numbers that are the roots of two transcendental equations in the form of the First Levy type auxiliary equation (11) in the x direction and the Second Levy type auxiliary equation (12) in the y direction, which is also known as the Modified Bolotin Method, which satisfies the conditions m ≤ p ≤ m+1 and n ≤ p ≤ n+1.

The First Auxiliary Levy Problem

$$-(k_1+k_2)\left(D_x\frac{d^4X_{mn}(x)}{dx^4}-2B\left(\frac{q\pi}{b}\right)^2\frac{d^2X_{mn}(x)}{dx^2}+D_yX_{mn}(x)\left(\frac{q\pi}{b}\right)^4\right)+G_s\left(D_x\left(\frac{d^6X_{mn}(x)}{dx^6}-\left(\frac{q\pi}{b}\right)^2\frac{d^4X_{mn}(x)}{dx^4}\right)\right)+2B\left(-\left(\left(\frac{q\pi}{b}\right)^2\frac{d^4X_{mn}(x)}{dx^4}+\left(\frac{q\pi}{b}\right)^4\frac{d^2X_{mn}(x)}{dx^2}\right)\right)+G_s\left(D_y\left(X_{mn}(x)\left(\frac{q\pi}{b}\right)^6+\left(\frac{q\pi}{b}\right)^4\frac{d^2X_{mn}(x)}{dx^2}\right)\right)-k_1k_2X_{mn}(x)+G_sk_1\left(\frac{d^2X_{mn}(x)}{dx^2}-X_{mn}(x)\left(\frac{q\pi}{b}\right)^2\right)=\rho h{\omega_{mn}}^2\left(k_1\left(\frac{d^2X_{mn}(x)}{dx^2}-\left(\frac{q\pi}{b}\right)^2X_{mn}(x)\right)-(-k_2+k_1)X_{mn}(x)\right) \tag{11}$$

The Second Auxiliary Levy Problem

$$-(k_1k_2)\left(D_x\left(\frac{p\pi}{a}\right)^4Y_{mn}(y)-2B\left(\frac{p\pi}{a}\right)^2\frac{d^2Y_{mn}(y)}{dy^2}+D_y\left(\frac{d^4Y_{mn}(y)}{dy^4}\right)\right)+G_s\left(D_xY_{mn}(y)\left(\left(\frac{p\pi}{a}\right)^6+\left(\frac{p\pi}{a}\right)^2\frac{d^4Y_{mn}(y)}{dy^4}\right)+2B\left(\left(\frac{p\pi}{a}\right)^4\frac{d^2Y_{mn}(y)}{dy^2}-\left(\frac{p\pi}{a}\right)^2\frac{d^4Y_{mn}(y)}{dy^4}\right)\right)+G_s\left(D_y\left(\frac{d^6Y_{mn}(y)}{dy^6}-\left(\frac{p\pi}{a}\right)^2\frac{d^4Y_{mn}(y)}{dy^4}\right)\right)-k_1k_2Y_{mn}(y)+G_sk_1\left(-\left(\frac{p\pi}{a}\right)^2Y_{mn}(y)+\frac{d^2Y_{mn}(y)}{dy^2}\right)=\rho h{\omega_{mn}}^2(k_1\left(-\left(\frac{p\pi}{a}\right)^2Y_{mn}(y)+\frac{d^2Y_{mn}(y)}{dy^2}-(k_1+k_2)Y_{mn}(y)\right) \tag{12}$$

2.4.1 Homogeneous Solution

Using the separation of variables method, two distinct equations will be obtained: the spatial solution W(x, y) comprising positional functions x and y, and the temporal solution T(t) as a function of time (t). Consequently, the homogeneous solution can be expressed as follows:

$$w_h=w(x,y,t)=\sum_{m=1}^{m=\infty}\ \sum_{n=1}^{n=\infty}\ [X(x)Y(y)]e^{-\xi\omega_{mn}t}[a_0cos(\omega_D)t+b_0sin(\omega_D)t] \tag{13}$$

2.4.2 Particular Solution

The particular solution is obtained from the plate's equation of motion, which incorporates the external load p(x, y, t) and the damping coefficient γ, thus, the equation can be expressed as follows:

$$w_p = w(x,y,t) = \sum_{m=1}^{\infty}\sum_{n=1}^{\infty}[X(x)Y(y)]\int_0^t \frac{e^{-\xi\omega_{mn}(t-\tau)}\, sin\, sin\, \omega_D(t-\tau)}{\rho h\, Q_{mn}\left[\frac{G_s}{k_1}\left(\frac{m^2\pi^2}{a^2}+\frac{n^2\pi^2}{b^2}\right)-\left(1+\frac{k_2}{k_1}\right)\right]}\int_0^a\int_0^b [X(x)Y(y)\left[\frac{G_s}{k_1}\nabla - \left(1+\frac{k_2}{k_1}\right)\right]p(x,y,\tau)dxdy]d\tau \quad (14)$$

2.5. Numerical parameter

In this numerical approach, six plate configurations are modelled with the geometries and mechanical properties of the materials presented in Table 1. And using concrete grade K 175, it has the strength to support loads of up to 14.5 MPa

Table 1. Plate Parameters

Notation			Unit
a	X Direction Length	15	m
b	Y Direction Length	7.5	m
h	Plate Thickness	15, 18, 20	cm
Ecx	X-Direction Plate Modulus of Elasticity	30 x 10^9	N/m^2
Ecy	Y-Direction Plate Modulus of Elasticity	20 x 10^9	N/m^2
vx	Poisson Ratio X Direction	0.15, 0.22	-
vy	Poisson Ratio Y Direction	0.10, 0.22	-
ρ	Plate Density	2400	kg/m^3
Dx	X-Directional Flexural Stiffness	$\frac{E_x h^3}{12(1+v_x v_y)}$	Nm
Dy	Y-Directional Flexural Stiffness	$\frac{E_x h^3}{12(1+v_x v_y)}$	Nm
B	Torsional Rigidity	$\sqrt{\boldsymbol{D_x D_y}}$	Nm
ξ	*Damping Ratio*	0,05	-

The following are the parameters used as parameters for modelling the blast load, which is assumed to occur above the plate in the middle of the span of the plate. The blast load is modelled as the local blast in Table 2.

Table 2. Blast Load Parameters

Notation			Unit
P_{max}	The maximum amplitude of the blast load	28.906	N/m^2
P_{min}	The minimum amplitude of the blast load	7.226,5	N/m^2
td0	Load start time	0	second
tdp	Positive phase	0,0018	second
tdn	Negative Phase	0,0036	second

The data taken in this study was correlated to obtain the values of k_1 as the 1st Spring Coefficient 1,626 x 10^6 N/m^2/m, k_2 as the 2nd Spring Coefficient 1,626 x 10^7 N/m^2/m, and G_s as Coefficient of Soil Shear in the soil, 2,85 x 10^5 N/m^2. The soil simulated in this study is a type of Soft from East Java, Indonesia.

3. Results and Discussion

3.1 Natural Frequencies

The natural frequency value of the system obtained from equation (5) for Figure 4(a) is 1143.55 rad/sec, while for Figure 4(b) the natural frequency value is 1111.9 rad/sec and for Figure 4(c) the natural frequency is 1081.32 rad/sec. For modes m = 4 and n = 4, the natural frequency value of the system in Figure 4(a) is 1612.52 rad/sec, for Figure 4(b), the natural frequency value is 1556.93 rad/sec and for Figure 4(c), the natural frequency is 1502.07 rad/sec. Likewise, for modes m = 4 and n = 5, the natural frequency value of the system for Figure 4(a) is 2247.9 rad/sec, while for Figure 4(b), the natural frequency value is 2163.61 rad/sec, and for Figure 4(c), the natural frequency is 2079.8 rad/sec. In m = 1 and n = 1 modes, the natural frequency value of the system for Figure 4. (f) is 1304.31 rad/sec, while for Figure 4(e) conditions, the natural frequency value is 586.926 rad/sec and for Figure 4(d) conditions, the natural frequency is 145.575 rad/sec. For modes m = 5 and n = 5, the natural frequency value of the system in Figure 4(f) is 2720.09 rad/sec, while for Figure 4(e) conditions, the natural frequency value is 2445.95 rad/sec and for Figure 4(d) conditions, the natural frequency is 2406.89 rad/sec.

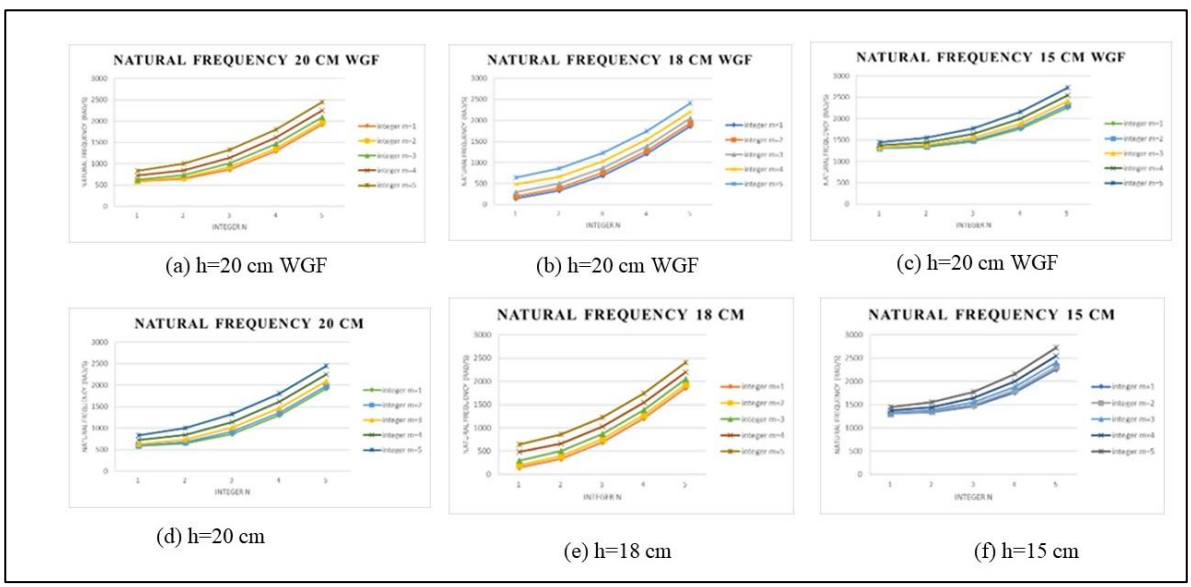

(a) h=20 cm WGF (b) h=20 cm WGF (c) h=20 cm WGF

(d) h=20 cm (e) h=18 cm (f) h=15 cm

Figure 4. Graph of natural frequency vibration variation of slab thickness with and without additional retrofitting using polyurea-infused woven glass fiber mesh composites

3.2 Maximum Absolute Deflection

The modeling in this study involves orthotropic slabs subjected to Friedlander blast loads with variations in slab thickness and additional retrofitting using polyurea-infused woven glass fiber mesh composites. The maximum deflection of the floor slab is calculated at the mid-span, where x = a/2 and y = b/2. Based on the results of the Maximum Absolute Deflection obtained from the Friedlander blast loading in all dimensions of the floor slab and blast duration, the overall values of the Maximum Absolute Deflection of the floor slab are consistent with the theory of small deflections. According to this theory, the maximum deflection that occurs must not exceed 10% or 1/10 of the slab thickness tested.

Table 4. Table of maximum absolute deflection for each slab thickness variation and added retrofitting

Type of Slab	Slab Thickness (cm)	Maximum Absolute Deflection	Percentage	Conclusion
Without Polyurea-infused Woven Glass Fiber Mesh Composites	15	0,00006696570	0,0133931%	compatible
	18	0,00000220558	0,0004411%	compatible
	20	0,00000899000	0,0017980%	compatible
With Polyurea-Infused Woven Glass Fiber Mesh Composites	15	0,00000159924	0,0003554%	compatible
	18	0,00000153336	0,0003195%	compatible
	20	0,00000220558	0,0004411%	compatible

The Maximum Absolute Deflection value, which represents the maximum deformation or displacement that occurs in the slab during the entire duration of the blast load (including the load start time, positive phase, and negative phase), is extremely small in the given data. For instance, it is 0,00006696570 for a slab of 15 cm thickness without additional retrofitting using polyurea-infused woven glass fiber mesh composites. However, for a slab of 20 cm thickness with additional retrofitting using the same material, the Maximum Absolute Deflection value is even smaller, at 0,00000220558. These minuscule values indicate that the slabs exhibit excellent resistance to blast loads, maintaining their structural integrity throughout the blast event. This suggests that the retrofitting technique employed in this study, possibly involving the use of polyurea-infused woven glass fiber mesh composites, is highly effective in enhancing the slab's blast resistance.

3.3 Time History

Time History Deflection is a graph that illustrates the relationship between slab deflection and the time during which the blast load occurred. Time history was analyzed with load parameters Pmax= 28.906 N/m^2, Pmin= 7226.5 N/m^2 and damping ratio ξ = 5%. The slab parameters analyzed are listed in Table 4.1. The time history of slab deflection for each slab thickness variation and additional retrofitting using polyurea-infused woven glass fiber mesh composites can be seen in the graph below:

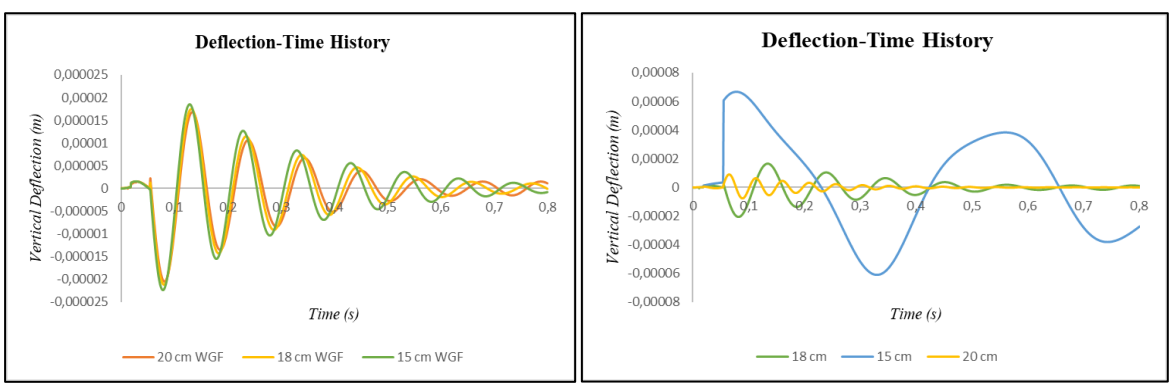

(a) (b)

Figure 5. (a) Time history of slab deflection for all slab thickness variations with additional retrofitting using polyurea-infused woven glass fiber mesh composites. (b) Time history of slab deflection all slab thickness variations without additional retrofitting using polyurea-infused woven glass fiber mesh composites

The graphs show that adding polyurea-infused woven glass fiber mesh composites to the retrofitting process makes the slab less likely to bend. Moreover, the deflection decreases with additional retrofitting using polyurea-infused woven glass fiber mesh composites. Additional retrofitting using polyurea-infused woven glass fiber mesh composites on slabs can significantly enhance their resistance to blast loads. This material adds strength and flexibility to the slabs, thereby better equipping them to withstand blast loads and reducing the deflection or deformation that occurs. Thickness variation also has a significant impact. Thicker slabs tend to have smaller deflections after being subjected to blast loads, regardless of whether additional retrofitting is applied. This is because thicker slabs have a greater capacity to withstand loads. However, with the addition of retrofitting using polyurea-infused woven glass fiber mesh composites, even thinner slabs can exhibit smaller deflections after being subjected to blast loads. This demonstrates that this material can improve the performance of slabs in withstanding blast loads, regardless of their thickness. The use of polyurea-infused woven glass fiber mesh composites in retrofitting can be an effective strategy for enhancing the resistance of structures to blast loads. Figure 6 presents a 3D visualization of deflection variations concerning slab types and slab thicknesses.

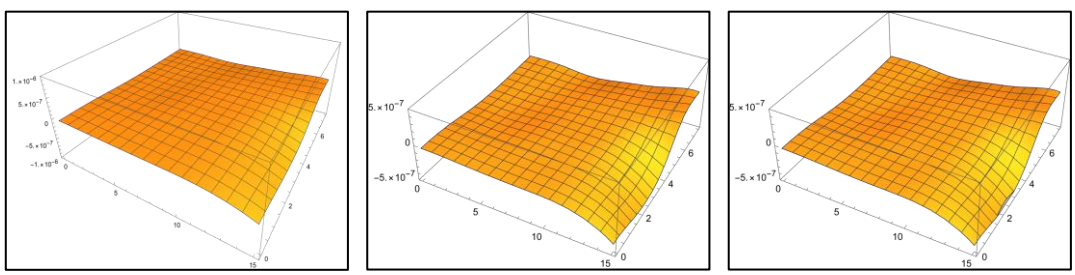

(a) *h*= 20 cm WGF (b) *h*= 18 cm WGF (c) *h*= 15 cm WGF

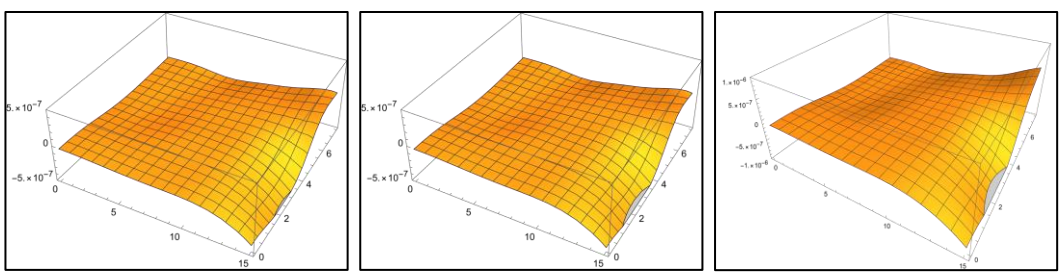

(d) *h*= 20 cm (e) *h*= 18 cm (f) *h*= 15 cm

Figure 6. 3D the slab region computed at t=0.015 s.

3.4 Moment

Larger deflections or deformations can happen on slabs with decreasing thicknesses (15 cm, 18 cm and 20 cm) if they are not retrofitted with polyurea-infused woven glass fiber mesh composites. This is due to the fact that thinner slabs have a lower capacity to withstand loads, including the moments generated by blast loads. However, if slabs of the same thickness (15 cm, 18 cm, and 20 cm) are given additional retrofitting using polyurea-infused woven glass fiber mesh composites, the deflection or deformation that occurs can be significantly reduced. This material adds strength and flexibility to the slabs, allowing them to withstand greater moments without significant deformation. In other words, the use of polyurea-infused woven glass fiber mesh composites in retrofitting can help mitigate the negative effects of greater moment values on slabs with decreasing thickness. This demonstrates the effectiveness of this material in enhancing the performance of slabs in withstanding blast loads.

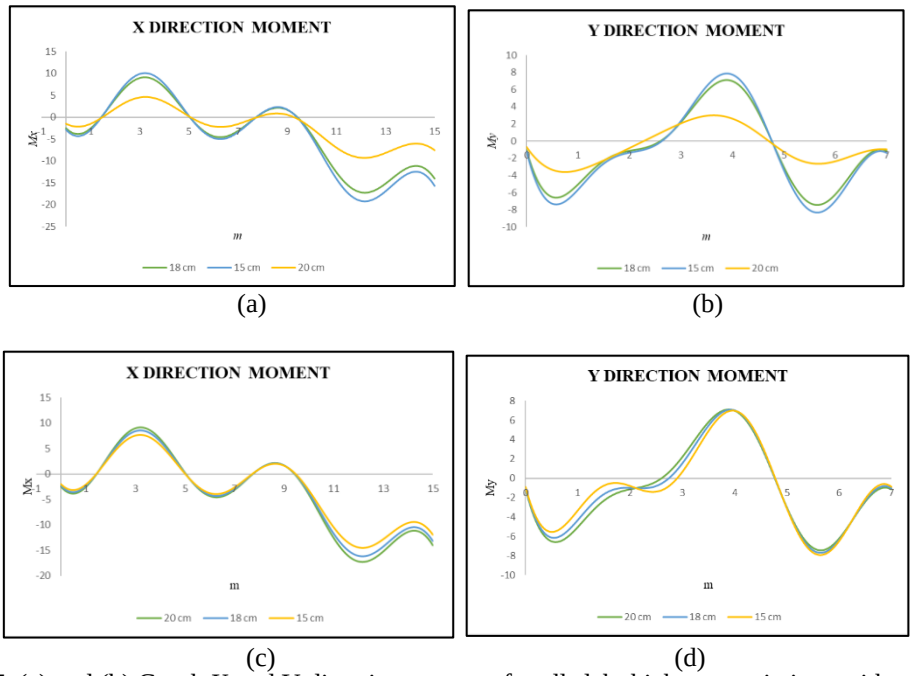

Figure 7. (a) and (b) Graph X and Y direction moment for all slab thickness variations with additional retrofitting using polyurea-infused woven glass fiber mesh composites. (c) and (d) Graph X and Y direction moment for all slab thickness variations without additional retrofitting using polyurea-infused woven glass fiber mesh composites

3.5 Flexural Stress Distribution

The stress distribution shows the maximum stress value on the slab. In the analysis of slab stress distribution, the data reviewed is the maximum normal stress distribution using the *Wolfram Mathematica* program. The type of slab was analyzed with three types of slab thickness, namely 15 cm, 18 cm and 15 cm, with and without additional retrofitting using polyurea-infused woven glass fiber mesh composites.

Table 5. Flexural Stress Distribution

Type of slab	Slab Thickness (cm)	Flexural Stress Distribution		
		Phase 1	Phase 2	Phase 3
Without Polyurea-Infused Woven Glass Fiber Mesh Composites	15	0,00067514100	0,00506562	0,0700449
	18	0,00049252300	0,00283288	0,0386509
	20	0,00026663200	0,0013317	0,0206311
With Polyurea-Infused Woven Glass Fiber Mesh Composites	15	0,00050824600	0,00277391	0,0378426
	18	0,00049743200	0,00280994	0,0383327
	20	0,00049252300	0,00283288	0,0386509

The Flexural Stress Distribution (the maximum normal stress distribution) during a blast load on a slab can be divided into three phases: phase 1 (load start time), phase 2 (positive phase), and phase 3 (negative phase). On a slab with a thickness of 15 cm without additional retrofitting using polyurea-infused woven glass fiber mesh composites, the flexural stress distribution values in phase 1, phase 2, and phase 3 are 0.00067514100, 0.00506562, and 0.0700449 respectively. These values indicate that the slab experiences relatively little flexural

stress during the blast load, even without additional retrofitting. However, on a slab of the same thickness (15 cm) with additional retrofitting using polyurea-infused woven glass fiber mesh composites, the flexural stress distribution values in phase 1, phase 2, and phase 3 are 0.00050824600, 0.00277391, and 0.0378426, respectively. These values are lower than those for the slab without retrofitting, demonstrating that the addition of retrofitting can lessen the flexural stress the slab experiences during the blast load. In other words, whether on thinner or thicker slabs, using polyurea-infused woven glass fiber mesh composites during retrofitting can help reduce the flexural stress the slab experiences as a result of a blast load. This demonstrates the effectiveness of this material in improving the performance of slabs in withstanding blast loads.

4. Conclusions

Based on the analysis conducted in the study Quantifying the Efficacy of Retrofitting Slabs Under Local Blast Loads through Numerical Analysis using Polyurea-Infused Woven Glass Fiber Mesh Composites, several conclusions can be drawn. Adding more retrofitting with polyurea-infused woven glass fiber mesh composites has the following effect on slabs that get thinner (15 cm, 18 cm, and 20 cm) without adding more retrofitting: Slabs with decreasing thickness and without additional retrofitting tend to experience larger deflections or deformations when subjected to blast loads. This is due to the lower capacity of the slabs to withstand loads, including the moments generated by blast loads. However, adding retrofitting using woven glass fiber mesh composites that are mixed with polyurea can make slabs that are getting thinner much more resistant to blast loads. This material adds strength and flexibility to the slabs, allowing them to better withstand blast loads and reduce the deflection or deformation that occurs. In other words, the use of polyurea-infused woven glass fiber mesh composites in retrofitting can help reduce the negative impact of slabs with decreasing thickness on blast loads. This demonstrates the effectiveness of this material in improving the performance of slabs in withstanding blast loads. Slabs with decreasing thickness (15 cm, 18 cm, and 20 cm) and without additional retrofitting tend to experience larger deflections or deformations when subjected to blast loads. However, adding retrofitting using woven glass fiber mesh composites that are mixed with polyurea can make slabs that are getting thinner much more resistant to blast loads. This demonstrates the effectiveness of this material in enhancing the performance of slabs in withstanding blast loads.

This is observed with parameters: maximum load Pmax = 28,906 N/m², minimum load Pmin = 7226.5 N/m², and damping ratio ξ = 5%. A conclusion can be drawn regarding the significant percentage decrease in the Maximum Absolute Deflection between with and without additional retrofitting using polyurea-infused woven glass fiber mesh composites. For instance, with a thickness of 15 cm, a substantial decrease is observed when additional retrofitting using polyurea-infused woven glass fiber mesh composites is applied with the same thickness, with a decrease value of 97.61%. Meanwhile, at a thickness of 18 cm, a decrease of 30.48% is experienced, and at a thickness of 20 cm, it is 70.40%. Based on the provided data, it can be concluded that the Flexural Stress Distribution (the maximum normal stress distribution) during a blast load on a slab varies depending on the slab thickness and whether additional retrofitting has been applied. The negative phase in the Friedlander load function influences the internal forces that occur in the slab. The design guideline is based on the theory of small deflections. According to this theory, the maximum deflection that occurs must not exceed 10% or 1/10 of the slab thickness being tested. The simulation in this paper is compatible with this criterion.

Acknowledgements

The authors would like to acknowledge Universiti Teknologi MARA, Shah Alam, Malaysia for assistance or encouragement from colleagues and Universitas Bakrie, Jakarta, Indonesia, for providing data support and assistance to complete this paper.

Declaration of Conflicting Interests

All authors declare that they have no conflicts of interest.

References

A. D. Kerr, "A study of a new foundation model," Acta Mechanica, vol. **1**, no. 2, pp. 135–147, 1965.

Abdelkrim K 2008 Stiffened Plates subjected to Uniform Blast Loading J. *of Civil Engineering and Management* **14** (3) 155-161

Alisjahbana, Sofia & Wangsadinata, Wiratman. (2008). Dynamic Response of Damped Orthtropic Plate on Pasternak Foundation to Dyanamic Moving Loads.

ASCE. Structural design for physical security, state of the practice; 1999.

Chundawat TS, Vaya D, Sini NK, Varma IK. Blast mitigation using FRP retrofitting and coating techniques. Polym Compos 2018;39(5):1389–402.

Ding C, Ngo T, Mendis P, Lumantarna R, Zobec M. Dynamic response of double skin façades under blast loads. Eng Struct 2016;123:155–65.

Guo Z, Xu Z, Chen C, Zhang B, Lehman DE, Cao S. Behavior of GFRP retrofitted reinforced concrete slabs subjected to conventional explosive blast. Mater Struct 2017;50(6):1–15.

Hajek R, Foglar M, Fladr J. Influence of barrier material and barrier shape on blast wave mitigation. Constr Build Mater 2016;120:54–64.

Ibrahim, M., Metwally. (2023). Damage assessment & innovation of efficient retrofitting solution of RC slabs exposed to contact explosion. Revista IBRACON de Estruturas e Materiais, doi: 10.1590/s1983-41952023000200007

J. T. Kenney, "Steady-state vibrations of beam on elastic foundation for moving load," J. Appl. Mech., **21**, 359–364 (1954).

Jacob N, Yuen S C K, Nurick G N, Bonorchis D, Desai S A and Tait D 2004 Scaling Aspects of Quadrangular Plates subjected to Localized Blast Loads-Experiments and Predictions Int. J. of Impact Engineering **30** (8-9) 1179-1208

Maji AK, Brown JP, Urgessa GS. Full-scale testing and analysis for blast-resistant design. J Aerosp Eng 2008;21(4):217–25.

Nam J-W, Kim H-J, Kim S-B, Yi N-H, Kim J-H. Numerical evaluation of the retrofit effectiveness for GFRP retrofitted concrete slab subjected to blast pressure. Compos Struct 2010;92(5):1212–22.

P. L. Pasternak, On a New Method of Analysis of an Elastic Foundation by Means of Two Constants, Gosudarstvennoe Izdatelstvo Literaturi po Stroitelstvu I Arkhitekture, Moscow, Russia, 1954.

Pham TM, Hao H. Review of concrete structures strengthened with FRP against impact loading. Structures 2016;7:59–70.

S. Alisjahbana and W. Wangsadinata, "Dynamic analysis of rigid roadway pavement under moving traffic loads with variable velocity," Interaction and Multiscale Mechanics, vol. **5**, no. 2, pp. 105–114, 2012.

S. Wolfram, Mathematica Reference Guide, Addison-Wesley, Redwood City, Calif, USA, 1992.

Sofia W A and Wiratman W 2014 Numerical Dynamic Analysis of Orthotropic Plates under Localized Blast Loading *ASEA SEC2, Bangkok*

US DEPARTMENT OF DEFENSE (DOD), "Unified Facilities CriteriaUFCDOD: Structures to Resist the Effect of Accidental Explosions", (2008),UFC 3-340-02, Washington, D.C.

US Department of the army. Structures to resist the effects of accidental explosions. Technical manual 5 1300; November 1990.

Yamaguchi M, Murakami K, Takeda K, Mitsui Y. Blast resistance of double-layered reinforced concrete slabs composed of precast thin plates. J Adv Concr Technol 2011;9(2):177–91.

Yi, Zhang., Jiahui, Hu., Feng, Hu., Xiao-hua, Yu. (2023). Numerical Simulation of the Blast Resistance of SPUA Retrofitted CMU Masonry Walls. Buildings, doi: 10.3390/buildings13020446